ADVANCED MATERIALS
www.advmat.de



# Barrierless Free Charge Generation in the High-Performance PM6:Y6 Bulk Heterojunction Non-Fullerene Solar Cell

*Lorena Perdigón-Toro, Huotian Zhang, Anastasia Markina, Jun Yuan, Seyed Mehrdad Hosseini, Christian M. Wolff, Guangzheng Zuo, Martin Stolterfoht, Yingping Zou, Feng Gao, Denis Andrienko, Safa Shoaee, and Dieter Neher**

**Organic solar cells are currently experiencing a second golden age thanks to the development of novel non-fullerene acceptors (NFAs). Surprisingly, some of these blends exhibit high efficiencies despite a low energy offset at the heterojunction. Herein, free charge generation in the high-performance blend of the donor polymer PM6 with the NFA Y6 is thoroughly investigated as a function of internal field, temperature and excitation energy. Results show that photocurrent generation is essentially barrierless with near-unity efficiency, regardless of excitation energy. Efficient charge separation is maintained over a wide temperature range, down to 100 K, despite the small driving force for charge generation. Studies on a blend with a low concentration of the NFA, measurements of the energetic disorder, and theoretical modeling suggest that CT state dissociation is assisted by the electrostatic interfacial field which for Y6 is large enough to compensate the Coulomb dissociation barrier.**

Organic solar cells (OSCs) have gained renewed interest with the emergence of non-fullerene acceptors (NFAs). Small molecule NFAs blended with donor polymers have rapidly advanced, reaching state-of-the-art power conversion efficiencies above 16%[1,2] for single junctions and 17.3% for all-organic solution-processed tandem cells.[3] These NFA-based blends benefit from a strong and redshifted absorption of the acceptor (A), complementary to the donor (D) absorption range, and small ionization energy offsets at the D/A heterojunction. As a direct consequence, short-circuit currents ($J_{SC}$) over 25 mA cm$^{-2}$ and open circuit voltages ($V_{OC}$) above 0.8 V have been reported for different NFA blends.[1,2,4,5] Notably, high $J_{SC}$ values have been shown for NFA-based blends with moderate energy offsets at the donor–acceptor heterojunction.[2,4,6] Low driving forces go along with reduced voltage losses, slightly above 0.5 V.[7–10] These new attributes and the remarkable efficiencies ask for a detailed analysis of the pathways of free charge generation.

Because of the low dielectric constant of organic semiconductors, photoexcitation creates strongly bound excitons. Therefore, photocurrent generation in OSCs comprises two steps. The first is charge generation, where a photogenerated exciton diffuses to the D/A interface to form an interfacial charge transfer (CT) state. This is followed by the second step, the dissociation of the CT into free carriers.[11] In the framework of Marcus theory, the efficiency of the first step, CT formation via interfacial charge transfer, is related to the so-called driving force for charge generation, $\Delta E_{S1,CT}$, which is the difference in energy of the intramolecular singlet ($S_1$) excited state on the donor or acceptor and the CT state.[12,13] Various recent publications deal with the efficiency and dynamics of charge generation in NFA blends, revealing efficient interfacial charge transfer also for small $\Delta E_{S1,CT}$.[7,14,15] Efficient charge generation has been rationalized by, e.g., favorable microelectrostatics.[16] In contrast, information on the dominant pathway and efficiency of the dissociation of the CT state to the fully charge separated state (CS) is rare for NFA-based blends. For homogeneous media, theory predicts a CT binding energy of around 400 meV,[17] in clear contrast to

L. Perdigón-Toro, C. M. Wolff, Dr. G. Zuo, Dr. M. Stolterfoht, Prof. D. Neher
Soft Matter Physics
Institute of Physics and Astronomy
University of Potsdam
Karl-Liebknecht-Str. 24-25, 14476 Potsdam-Golm, Germany
E-mail: neher@uni-potsdam.de

The ORCID identification number(s) for the author(s) of this article can be found under https://doi.org/10.1002/adma.201906763.



**DOI: 10.1002/adma.201906763**

L. Perdigón-Toro, S. M. Hosseini, Prof. S. Shoaee
Disordered Semiconductor Optoelectronics
Institute of Physics and Astronomy
University of Potsdam
Karl-Liebknecht-Str. 24-25, 14476 Potsdam-Golm, Germany

H. Zhang, Prof. F. Gao
Department of Physics
Chemistry and Biology (IFM)
Linköping University
581 83 Linköping, Sweden

Dr. A. Markina, Dr. D. Andrienko
Max Planck Institute for Polymer Research
Ackermannweg 10, 55128 Mainz, Germany

Dr. J. Yuan, Prof. Y. Zou
College of Chemistry and Chemical Engineering
Central South University
Changsha 410083, P. R. China

 

the high external quantum efficiency (EQE) for photocurrent generation of many NFA-containing devices. Several studies showed high EQE to be related to a larger driving force.[15,18–20] This situation reminds of the "hot" dissociation model, where exciton dissociation creates a more loosely bound electronically/vibronically excited CT state.[21,22] A popular method to address this issue is to measure the photocurrent response as a function of excitation energy, comprising the spectral range which only excites low lying CT states. Interestingly, measurements on fullerene-based blends gave evidence for a cold dissociation pathway, which involves an equilibrated CT state manifold.[23,24] An elegant approach to study the binding of the involved CT state is to measure the temperature dependence of CT dissociation. Notably, the activation energy for CT dissociation is unaffected by entropic effects.[25] Temperature-dependent studies on fullerene-based blends revealed activation energies for CT dissociation from few tens to ≈100 meV,[25–29] with some important exemptions as discussed next. We are aware of only one publication reporting temperature-dependent measurements on the CT binding in a NFA blend.[30] Here, pump-push photocurrent spectroscopy (PPPc) was applied to a blend of the donor PffT4T with the NFA EH-IDTBR, suggesting a CT binding energy of 100 meV. This blend exhibits very small energy offset of the lowest unoccupied molecular orbitals (LUMOs) and of the highest occupied molecular orbitals (HOMOs) at the D/A heterojunction of only 0.21 and 0.24 eV, respectively, suggesting a small (or even negligible) $\Delta E_{S1,CT}$. While the value of $\Delta E_{S1,CT}$ primary dictates the efficiency of charge generation, it is also expected to affect the dissociation of the formed CT state. For example, increasing the CT state energy will go along with the suppression of vibronic coupling to the ground state, thereby reducing the nonradiative CT decay rate as the competing process to CT dissociation.[31,32] In agreement to this, recent work on low donor content blends revealed a power-law dependence of the CT dissociation efficiency on the energy of the lowest CT state.[33] We, therefore, expect that in NFA-based blends, the benefit of a smaller energy driving force and higher lying CT state manifold is not only an increased $V_{OC}$ but also a more efficient CT dissociation, due to slower geminate recombination. However, when the CT approaches the $S_1$, electronic coupling may result in the formation of hybridized states with mixed exciton-CT character.[13,34] Following this rational, recent work predicted a stronger binding and faster geminate recombination of such mixed states to the ground state, thereby reducing the efficiency of CT dissociation.[32,35,36]

In this work, we perform a comprehensive study of free charge generation and of nongeminate losses in a state-of-the-art NFA blend with a low driving force, using a combination of temperature-dependent time-delayed collection field (TDCF), EQE, and $V_{OC}$ measurements. Our system of choice is the wide bandgap polymer PM6, based on a fluorinated-thienyl benzodithiophene (BDT-2F) unit, and the small molecule Y6, which contains a dithienothiophen[3.2-b]-pyrrolobenzothiadiazole (TPBT) central fused unit flanked with 2-(5,6-difluoro-3-oxo-2,3-dihydro-1H-inden-1-ylidene)malononitrile (2FIC) units (chemical structures shown in **Figure 1**a). PM6:Y6 devices have been reported to exhibit a power conversion efficiency (PCE) of up to 15.7% despite a relatively low ionization energy (IE) offset for hole transfer (see Figure 1a).[4] Given the broad absorption spectrum and the large difference of the $S_1$ energies of the donor and acceptor, the PM6:Y6 blend is a relevant system for the study of free charge generation in relation to excess energy and driving force. Our experiments show that the efficiency of free charge generation is independent of the electric field regardless of whether the donor, the acceptor, or states in the tail of the blend absorption are excited. Temperature-dependent optoelectronic studies reveal nearly barrierless free charge formation. Our experimental findings are consistent with theoretical modeling which reveals an electrostatic interfacial field which for Y6 is large enough to compensate the Coulomb dissociation barrier.

All of our studies were performed on optimized PM6:Y6 (1:1.2, w/w) blends in an inverted solar cell geometry, given the superior stability of this device architecture under prolonged pulsed laser illumination. Table S1 (Supporting Information) contains the averaged photovoltaic parameters of devices prepared in this work. Our devices exhibit a PCE of 13.7%, which is ≈10% smaller than the PCE of 15.3% as reported by Yuan et al. for the as-cast blend in the conventional device architecture.[4] Inspection of the photovoltaic parameters (*PV*) shows that the difference originates mainly from a lower $J_{SC}$ (22.4 mA cm$^{-2}$ in our as-cast 100 nm inverted devices vs 24.3 mA cm$^{-2}$ in 150 nm regular devices), while differences in the fill factor (FF) and $V_{OC}$ are minor. This suggests that our cells suffer mainly from a less efficient photon absorption and/or exciton harvesting, while all other processes are virtually the same as in the blend reported by Yuan et al. Remarkably, we were able to upscale the devices to an active area of 1 cm$^2$ with only ≈2% losses in FF (see Figure S1, Supporting Information, for the *PV* parameters and Figure S2, Supporting Information, for the current density–voltage (*J*–*V*) characteristics of a 1.0229 cm$^2$ area certified cell). This cell delivered a PCE of 13.45%—the highest certified value reported so far for a >1 cm$^2$ single-junction OSC device.[37]

Figure 1a shows the energy diagram as derived from cyclovoltametric measurements on films of the neat materials in ref.[4] (see Note S1, Supporting Information). As a consequence of the small IE offset of only 0.09 eV, we expect a small driving force $\Delta E_{S1,CT}$. Figure S3 (Supporting Information) shows the comparison of the sensitive external quantum efficiency ($EQE_{PV}$) of the pristine NFA and the blend where we indeed observe very little difference between the spectra. However, the electroluminescence (EL) spectra of PM6:Y6 display low energy features which could indicate the presence of CT state emission (see Figure S4, Supporting Information). To determine the CT energy, we fitted the reduced $EQE_{PV}$ and EL spectra following the approach by Vandewal et al.[38] The resulting $E_{CT}$ = 1.41 eV is consistent with the value taken from the maximum of the derivative of the $EQE_{PV}$ curve,[39] as also shown in Figure S4 (Supporting Information). Alternatively, we fitted only the low energy shoulder of the EL spectra using Marcus theory (as previously done in the work by Tang et al.[18]) which yields $E_{CT}$ = 1.29 eV. The singlet exciton energy of PM6 and Y6 were obtained from the crossing point of the absorption and photoluminescence (PL) spectra of the pristine films. This gives an energy of the lowest excited singlet exciton $S_1$ of 1.90 eV for PM6 and of 1.42 eV for Y6 (Figure S4, Supporting Information). Conclusively, the driving force for charge generation through channel I (electron transfer) is $\Delta E_{S1(D),CT} \cong 0.60$ eV, while it is much smaller through channel II (hole transfer), with an estimated $\Delta E_{S1(A),CT} \leq 0.13$ eV.

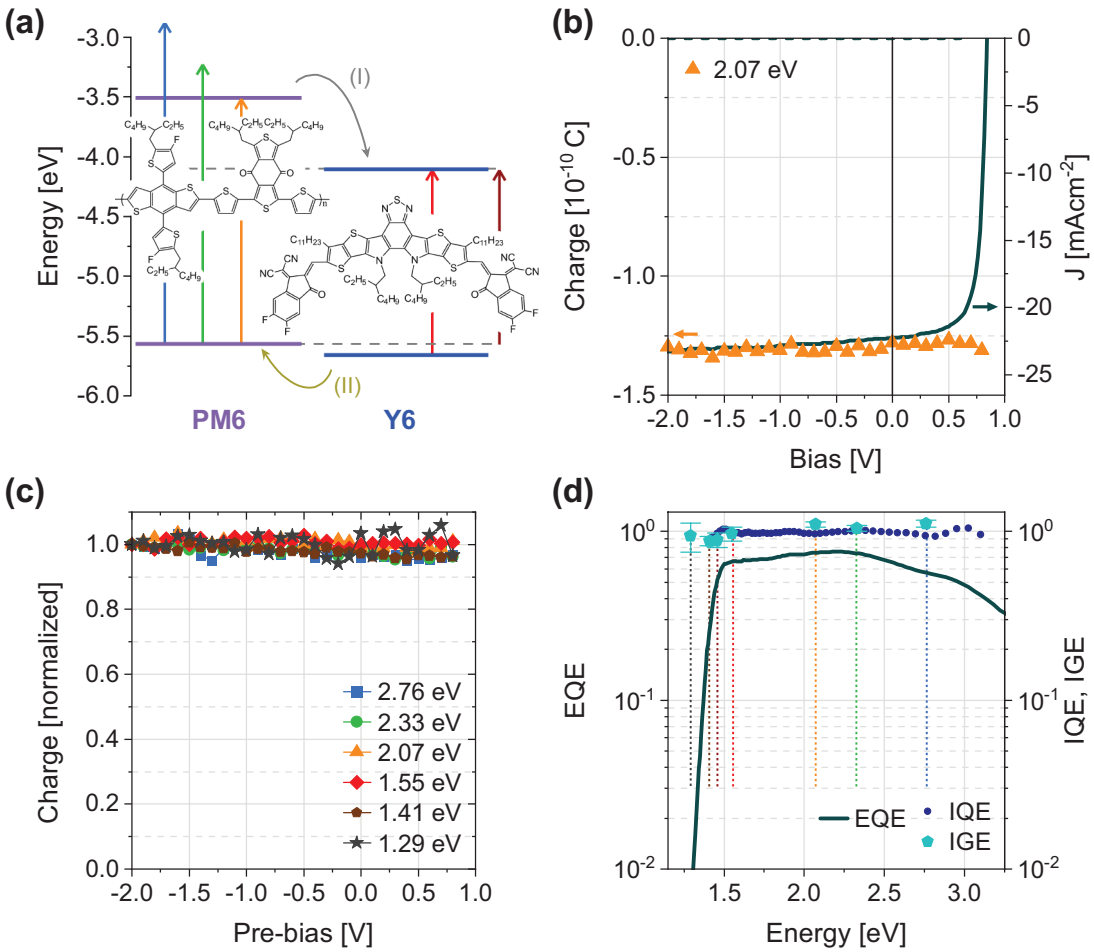


**Figure 1.** a) Chemical structure of PM6 and Y6 and energy levels measured by cyclic voltammetry, taken from ref. [4]. The curved arrows indicate the pathways for charge generation via electron transfer (channel I) or hole transfer (channel II), respectively. b) Bias-dependent free charge generation (symbols, left axis) for an inverted PM6:Y6 device measured by TDCF for an excitation of 2.07 eV with a low fluence of 0.05 μJ cm$^{-2}$ and $V_{coll}$ = −2.5 V. For comparison, the current density–voltage characteristics of the device under simulated AM1.5G light is also shown (solid lines, right axis). c) Total charge $Q$ as a function of pre-bias ($V_{pre}$) normalized to the value at −2 V for energies corresponding primarily to PM6 excitation (2.76, 2.33, and 2.07 eV), Y6 excitation (1.55 and 1.41 eV), and CT state excitation (1.29 eV). d) EQE (left axis) experimentally measured for a PM6:Y6 device and IQE and IGE (right axis) as optically modeled from EQE and TDCF results, respectively.

In order to elucidate the role of the pathways on the free carrier generation, we performed TDCF experiments as a function of the electric field and temperature with excitation at different photon energies. The experimental details on TDCF have been described elsewhere.[29,40] In short, the device is excited with a short laser pulse (≈5 ns) while being held at a given pre-bias ($V_{pre}$). After a delay time of 6 ns charges are extracted by applying a high reverse collection bias ($V_{coll}$). To ensure that nongeminate losses are insignificant during the measurement, we apply a sufficiently large $V_{coll}$ of −2.5 V and the laser intensity is chosen to lie in the linear regime (the extracted charge is strictly proportional to the laser fluence). Then, the total extracted charge ($Q$) is a direct measure of the efficiency of free charge generation under these conditions.

Figure 1b shows the results of such a measurement, where $V_{pre}$ is swept from reverse bias to $V_{OC}$. Here, the excitation energy was 2.07 eV which excites primarily the donor polymer at its low energy absorption maximum (see the absorption spectra of donor, acceptor, and the blend in Figure S5, Supporting Information). We find that the total charge $Q$ does not depend on the applied bias $V_{pre}$, even when $V_{pre}$ approaches $V_{OC}$, meaning that the photocurrent does not suffer from increased geminate recombination when decreasing the internal field. Theory predicts that an appreciable barrier for CT dissociation would cause a dependence of the dissociation efficiency on the electric field because of electrostatic barrier lowering.[11,41] Any gradient of the $J$–$V$ at $J_{SC}$ (green solid line and right axis in Figure 1b) must, therefore, originate from bias-dependent nongeminate recombination (NGR), which will be addressed later in this work.

Figure 1c assembles the result of bias-dependent TDCF generation experiments for different excitation energies, ranging from 2.76 eV to excite a high energy exciton state manifold down to 1.29 eV, which is within the low energy shoulder of the EL spectra attributed to emission from the CT state (refer to Figure S4, Supporting Information). With this, our experiments

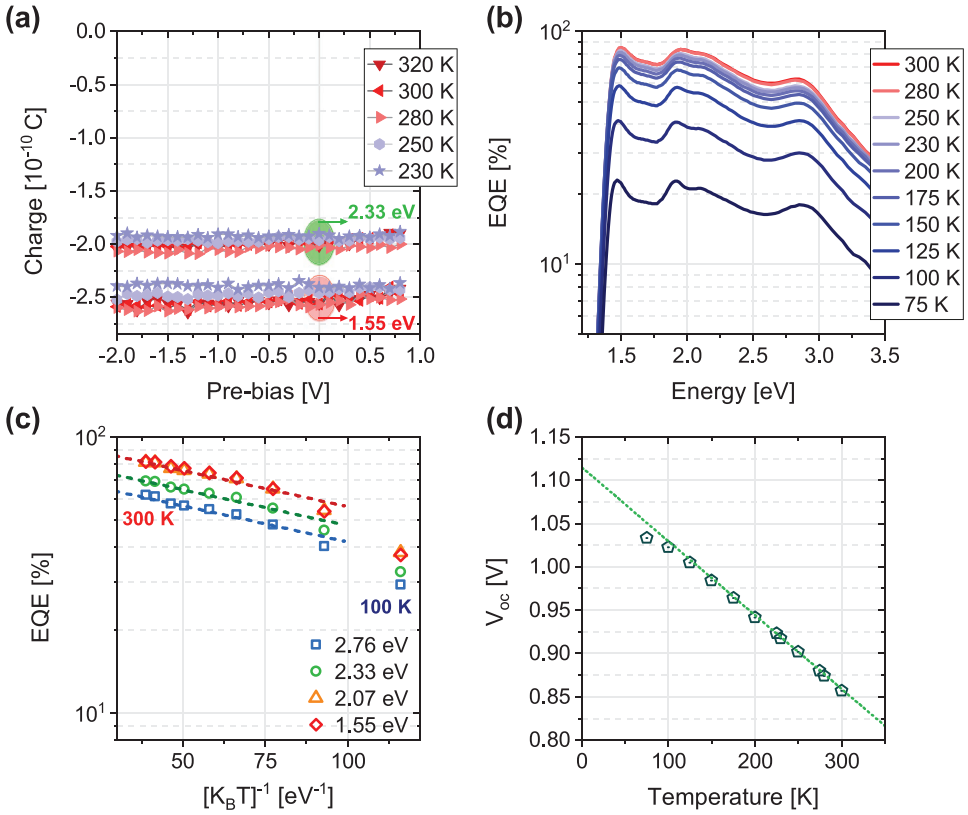


**Figure 2.** a) Bias-dependent free charge generation for a PM6:Y6 device measured at different temperatures by TDCF (with a fluence of 0.1 μJ cm$^{-2}$ and $V_{coll}$ = −2.5 V). The excitation was chosen to excite exclusively Y6 at 1.55 eV or both components at 2.33 eV. b) External quantum efficiency at different temperatures measured at short-circuit conditions and low intensity. c) Temperature dependence of EQE values at different excitation energies. Open symbols correspond to the raw data and the dashed lines are fits to Equation (1) with a calculated $E_a$ = 6 meV for all excitation energies. d) Temperature dependence of $V_{OC}$. The linearity of the plot reveals that the free carrier density in the device remains essentially constant down to a temperature of ≈100 K.

cover an exceptional wide range in photon energy, including predominate channel I and channel II excitation, hot exciton creation, or the direct formation of CT states. Clearly, charge generation is field-independent for all used excitation energies, irrespective of the predominant channel of charge transfer or whether we excite directly the CT state. To complement this finding, we calculated the internal quantum efficiency (IQE) spectra of PM6:Y6 from the experimental EQE spectrum by taking the reflection ($R$) and parasitic absorption (PA) losses in the device stack (i.e., IQE = EQE/(1−$R$−PA))[42] into account (see Note S2 and Figure S6, Supporting Information, for further details on the procedure). Note that the main source of PA in the considered photon energy range is by the $MoO_3$ layer. The same procedure was applied to the TDCF data to determine the internal generation efficiency (IGE), which is the number of generated free charges per absorbed photon. As shown in Figure 1d, both IQE and IGE are independent of excitation energy and are close to unity. This has important implications. First, free charge generation does not benefit from a larger driving force (channel I vs channel II) nor from excess photon energy. These findings substantiate the conclusions from earlier studies on fullerene-based solar cells, which were interpreted in terms of a cold generation process, involving a low energy CT state manifold as a precursor to free charges.[23,29,42] Second, the lack of a field dependence of generation, independent of the excitation energy, suggests a low energetic barrier for the dissociation of such low energy precursor states. Third, with IQE and IGE being close to one, losses due to exciton harvesting, geminate recombination, or charge extraction must be very small. This points to an ideal morphology, where the domains of the phase separated blend allow all photogenerated excitons to diffuse to the donor–acceptor interface, while a good interpenetration of donor- and acceptor-rich regions prevents trapping of photogenerated charges on isolated domains.[43] Indeed, recent work by Chandrabose et al.[44] reported an exceptionally high exciton diffusion coefficient in well-ordered domains of a NFA, which was assigned to the rigid nature of the molecule and low energetic disorder. We finally note that optical modeling shows the EQE (and $J_{SC}$) of our inverted device to be significantly affected by reflection and parasitic absorption, causing the PCE to lie below published PM6:Y6 record values.

**Figure 2**a shows the results of temperature-dependent TDCF experiments at 1.55 eV, exciting exclusively the NFA at its absorption maximum and at 2.33 eV, which excites both components of the blend. We observe that cooling down the device to 230 K has essentially no effect on the efficiency of charge generation and that it remains field independent even for the lowest temperature tested. The same holds for other excitation

energies (Figure S7, Supporting Information). Figure S8 (Supporting Information) plots the results from Figure 2a as function of temperature, normalized to the value at 320 K, where we observe a less than 10% drop of the free charge generation efficiency when decreasing the temperature from 320 to 230 K. This suggests a very small (if any) barrier toward CT dissociation. To substantiate this finding, our TDCF results were complemented by taking EQE spectra at different temperatures, with results shown in Figure 2b. Those measurements were performed at low intensity to avoid second-order losses (i.e., recombination of free charge carriers), meaning any losses in the EQE should be mainly geminate.[26] We observe a gradual but only weak decrease of the EQE down to $T \cong 150$ K, followed by a steeper drop when decreasing the temperature further, possibly related to charge transport issues. Notably, changing the temperature leaves the shape of the spectrum essentially unaffected down to ≈125 K (see Figure S9, Supporting Information). To extract an activation energy ($E_a$) for photocurrent generation, we plotted the EQE versus $(k_B T)^{-1}$ according to

$$\mathrm{EQE} = \mathrm{EQE}_0 \exp\left(-\frac{E_a}{k_B T}\right) \quad (1)$$

using EQE values at the same energies as measured by TDCF. Here, $\mathrm{EQE}_0$ is the EQE at infinite temperature. The result is depicted in Figure 2c, together with fits of Equation (1) (dashed line) to the high temperature region. The analysis yields a very small activation energy $E_a$ of only 6 meV for all excitation energies, confirming our conclusion from TDCF that charge generation at RT in this high-performance blend is essentially barrierless.

As outlined earlier, there is a more pronounced effect of temperature on the EQE below ≈150 K, which we propose to be caused by increased nongeminate recombination due to extraction issues, but whose origin may also lie in the onset of geminate recombination. To address this issue, we performed measurements of the $V_{OC}$ over a wide temperature range, following the routine proposed by Gao et al.[26] At open-circuit conditions, generation equals recombination and extraction does not obscure the interpretation of the results (see Note S3 and Figure S10, Supporting Information). Figure 2d shows the resulting data for an illumination intensity equivalent to 1 sun. The $V_{OC}$ increases in a linear fashion with the temperature down to ≈100 K, which rules out an appreciable effect of temperature on the free carrier density for this temperature range. Conclusively, the above measurements reveal efficient free charge generation down to ≈125 K with an activation energy below 10 meV, ruling out a significant barrier for charge separation in PM6:Y6.

As pointed out above, studies with different methods and on different blend systems revealed values for the activation energies of CT dissociation between few tens of meV to ≈100 meV.[25–29] A notable exemption is the annealed blend of P3HT with PCBM for which barrierless free charge generation was consistently shown.[45] This blend stands out by the strong tendency of the constituting components to phase-separate into well-crystallized domains but also by its large driving force of 0.9 eV.[46] A second example where a very low temperature dependence of CT dissociation was being proposed is the blend of TQ1 with PCBM.[47] This blend exhibits a reasonably large $\Delta E_{S1,CT}$ (>0.2 eV),[48] but more importantly a large energetic disorder of the ionization energy (IE) and the electron affinity (EA).[49]

This important finding raises the question about the origin of the processes compensating the unavoidable Coulomb attraction between the electron and the hole of the geminate pair in our PM6:Y6 blend. It has been argued that CT separation can be assisted by various processes (besides the driving force defined previously) such as entropy,[50,51] high local mobilities,[52,53] and delocalization of charges on aggregated phases of the donor and/or the acceptor.[25,54–59] In addition, several recent papers highlighted the role of energetic disorder in providing low energy sites for the dissociation of CT states in D/A blends or even for singlet excitons in neat organic semiconductors.[25,50,60,61] For instance, Hood and Kassal[50] concluded that a Gaussian disorder $\sigma$ of 100 meV is sufficient to reduce the free-energy barrier to ≈25 meV, meaning that thermal energy can be sufficient to dissociate CT states at room temperature. Accordingly, we performed a temperature-dependent study of space-charge limited currents (SCLC) in electron- and hole-only devices to quantify the energetic disorder in the PM6:Y6 blend (see Figure S11, Supporting Information). The data were modeled with 1D drift-diffusion simulations based on the extended Gaussian disorder model, according to Felekidis et al.[62] We found the energetic disorder of the IE to be $\sigma_{IE} = 83$ meV and that of the EA, $\sigma_{EA} = 71$ meV. That the $\sigma$ is lower for electrons in the LUMO of Y6 confirms conclusions from GIWAXS measurements by Yuan et al.,[4] that the NFA forms well-ordered domains in the blend. Such small values for $\sigma$ exclude energetic disorder as the main driving force for charge separation. Note that the study on barrier lowering in ref.[50] includes the combined effect of energetic disorder and of entropy, while the activation energy for CT dissociation is unaffected by entropic effects.[25]

It has been argued that SCLC measurements are not well suited to study the density of states (DOS) that is involved in the photogeneration process.[63] This is because SCLC is by the motion of dark-injected charges, which are situated in the tail of the DOS right from the beginning, while photogenerated charges may initially occupy states near the center of the DOS. We have recently shown that studies of dispersive recombination with TDCF provide direct access to the thermalization properties of photogenerated carriers in the actual device.[40,64,65] For this measurement, the device is held at a given $V_{pre}$, typically close to the maximum power point, while the delay time ($t_{del}$) is now varied from few ns to µs (see Note S4, Supporting Information). Figure S12 (Supporting Information) shows the total extracted charge carrier density $n_{tot}$ as a function of $t_{del}$ at different excitation fluences, where the differential of $n_{tot}$ over time is the free charge recombination rate $R$. There is a significant acceleration of recombination with increasing fluence, meaning that recombination is a higher order process. To gain information on how the rate depends on carrier density and time, $R$ is plotted as a function of the charge carrier density $n_{coll}$ present in the sample at $t_{del}$, with the result shown in **Figure 3**a. Except for some tailing at low fluences and early times, we observe that all $R(n_{coll}, t_{del})$ data fall onto one line, independent of the initial fluence, and this line has a slope of two in the log-log plot. This proves that $R$ does not explicitly depend on $t_{del}$ and that nondispersive bimolecular recombination of free charges in the bulk of

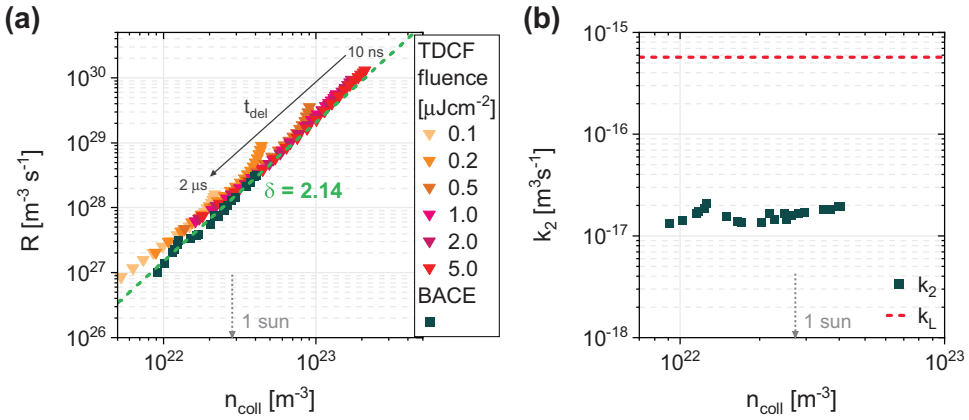


**Figure 3.** a) Recombination rate versus photogenerated charge carrier density. For TDCF measurements (triangles), $R$ is plotted as function of the remaining charge in the device ($n_{coll}$) after a given certain delay time ($t_{del}$). Squared data depict steady-state recombination from BACE experiments, and the dashed line is a fit to a power law-type dependence of the recombination rate on the carrier density, with a recombination order of 2.14. b) Bimolecular recombination coefficient as function of charge carrier density calculated from the BACE data via $R = k_2 n^2$. For comparison, the dashed red line shows the recombination coefficient $k_L$ as predicted by Langevin recombination.

the blend is the predominant mechanism in this blend.[64,66] The situation is clearly different from donor–acceptor blends with large energetic disorder, such as TQ1:PCBM, where recombination was found to be dispersive up to the microsecond time range.[40,65] We have complemented this transient study by investigating the recombination properties under steady-state conditions, using bias assisted charge extraction (BACE) (Note S5, Supporting Information, contains further details on the measurement).[67,68] The results are included as squares data points in Figure 3a for direct comparison to TDCF. These steady-state recombination data lie exactly on the results from TDCF, meaning that recombination involves the same site distribution, from the nanosecond timescale to steady state. The dashed line corresponds to a fit to the power law-type dependence of the recombination rate on the carrier density, with a recombination order of $\delta = 2.14$. A recombination order close to 2 rules out trap-assisted recombination.[69,70] The analysis of the recombination data according to $R = k_2 n^2$ yields a bimolecular recombination coefficient $k_2 = 1.7 \times 10^{-17}$ m$^3$ s$^{-1}$, depending only weakly on charge carrier density, as shown in Figure 3b. We also examined the dependence of the carrier density and the recombination current on $V_{OC}$, which gave an ideality factor $n_{id}$ of 1.17 and an $m$-factor of 1.18 (see Figure S13, Supporting Information, for details). Hofacker and Neher[64] have recently analyzed how the exact values of $\delta$, $n_{id}$, and $m$, depend on the shape of the DOSs and the predominant recombination pathway. The presented data strongly support that nongeminate losses occur exclusively through recombination of carriers situated in a narrow Gaussian DOS.

Our results question energetic disorder and charge thermalization in a broad DOS as the origin of efficient free charge generation in our PM6:Y6 blend. It has been recently proposed that an aggregation-dependent electron affinity causes an energy cascade which drives electrons out from the more disordered D/A heterojunction into the well-crystallized domains of neat NFA.[71] Also, measurements of the activation energy for CT dissociation for different blends revealed a direct correlation with the nanomorphology, while there was no consistent dependency on the driving force.[27,29] We have so far observed strong evidence of NFA aggregation, such as the strong redshift in absorption for films, the small energy shift from $EQE_{PV}$ to electroluminescence emission, and the low energetic disorder in the EA. A recent study of the morphology of PM6 blended with Y6 revealed phase separation into well-crystallized domains with an average domain size of ≈20 nm.[72] In order to elucidate the role of NFA aggregate formation on the efficiency of free charge generation, additional experiments were performed on "diluted" low-acceptor-content PM6:Y6 (10:1, w/w) blends. Evidence for the deaggregation of Y6 comes from the marked blueshift of the NFA absorption and photoluminescence in the dilute blend compared to the 1:1.2 ratio and the neat acceptor layer (see Figure S14, Supporting Information). TDCF experiments on such a dilute blend revealed a pronounced effect of the electric field on the photogeneration efficiency (Figure S15, Supporting Information), where larger geminate losses appear at lower fields. The even stronger effect of bias on the steady-state photocurrent points to additional nongeminate losses, which we attribute to slow electron extraction in combination with a significant faster rate for NGR (see the results of TDCF recombination studies on the dilute blend in Figure S16, Supporting Information). Notably, free charge generation in this dilute acceptor blends is temperature dependent, with an activation energy of ≈22 meV (Figure S17, Supporting Information).

We now discuss the potential microscopic mechanism of barrierless charge generation in the optimized PM6:Y6 blend. As we have already mentioned, charge separation involves two steps: exciton dissociation into a CT state and the subsequent dissociation of that CT state into a free electron–hole pair. Since the PM6:Y6 donor–acceptor interface has a sufficiently large driving force between the excited donor/acceptor (D*/A*) and the CT state (≈0.61 eV for the D* and 0.13 eV for the A*), the transition from the D*/A* states to the CT state is barrierless. On the other hand, we expect the Coulomb binding energy between the CT and charge separated (CS) states to be of the order of 0.4 eV.[17] Our temperature-dependent measurements, however, show that charge separation is barrierless in our PM6:Y6 blend.

To understand this, we first point out that because of the phase-separated structure the electrostatic potential at a D/A

interface can have a pronounced bend due to a molecular concentration gradient.[73] This concentration gradient modulates the solid-state crystal field around the charge.[74–76] In other words, a hole away from the interface interacts with a smaller density of acceptors dispersed in the donor phase. For the acceptor–donor–acceptor molecular architecture of Y6, the electrostatic potential, termed here as a bias potential $B$, has a sign which pushes electrons and holes away from the interface. Another important implication of such bias potential is that it reduces the energetic difference between the CT and CS states, thus enabling the barrierless CT state dissociation.[73] Therefore, the bend of the bias potential may compensate, at least partially, the Coulomb attraction of the CT state.

An exact evaluation of the bias potential requires the knowledge of an atomically resolved donor–acceptor interface. Simulating such interfaces is computationally demanding, and here we provide only an upper bound for the bias potential, by assuming that in a CT state a hole on a donor molecule is dressed by the acceptor crystal field and vice versa. The crystal fields are evaluated using the polarizable force-field tailored specifically for Y6[77,78] (see Note S6 and Figure S18, Supporting Information for details). The estimated $B$ value for Y6 is 1.1 eV. According to recent simulation work, barrierless CT dissociation requires $B > 1$ (unpublished). The large positive bias can be clearly traced back to the Y6 A-D′-A″-D′-A molecular architecture, which leads to a large static quadrupole moment of a molecule ($Q_{xx} = -120$, $Q_{yy} = 80$, $Q_{zz} = 40$ D Ä) and hence large crystal fields, as shown in **Figure 4**a. Note that the molecular dipole moments cancel out due to the dimerization in a unit cell, as shown in Figure S19 (Supporting Information). Absence of a unit cell dipole and high crystallinity of Y6 films also imply its relatively narrow density of states, which is shown in Figure 4b. Measured and calculated DOS widths exclude effects of nonequilibrium relaxation of charges which could assist charge splitting. Note that the electron affinity and ionization energy are both within the "trap-free" window, hinting at a trap-free ambipolar transport in pristine Y6 films.[79,80] In addition, the calculated excited state reorganization energy of Y6 has a very small value of 0.24 eV, which promotes large exciton diffusion rates and lengths and makes it less sensitive to the morphological variation in a bulk heterojunction.

With the exceptional free charge generating properties in PM6:Y6 demonstrated, the efficiency of our devices is mainly limited by insufficient photon absorption and free charge extraction. Our time-resolved and steady-state measurements showed consistently that nongeminate recombination is bimolecular in nature, with a NGR coefficient $k_2 = 1.7 \times 10^{-17}$ m$^3$ s$^{-1}$ at 1 sun illumination conditions. This value needs to be compared to the charge encounter rate according to the Langevin model, giving $k_L = 5.5 \times 10^{-16}$ m$^3$ s$^{-1}$, shown by a dashed line in Figure 3b (see also Note S7 and Figure S21, Supporting Information, for more details). The comparison shows that NGR is not largely suppressed in our blend. Recently, impedance spectroscopy on PM6:Y6 reported a $k_2$ of 3–5.8 $\times 10^{-19}$ m$^3$ s$^{-1}$.[81] These measurements were performed on a regular device geometry, with a poly(3,4-ethylenedioxythiophene)polystyrene sulfonate (PEDOT:PSS) bottom electrode. The lower $k_2$ reported in ref. [81] may result from a specific blend morphology, due to a different bottom electrode. To ensure that our measurements on inverted devices are not affected by the choice of the bottom electrode, we studied the steady-state nongeminate recombination in a regular device (PEDOT substrate electrode) using BACE (see Figure S22, Supporting Information). This device had a PCE of 14.7%. Within the uncertainty of the experiment both device geometries exhibit the same order and coefficient of recombination. Since nongeminate recombination is highly sensitive to the blend morphology,[82] we conclude that the bulk properties are depending only little on the bottom electrode.

The efficiency limitation that comes with a high $k_2$ value can be illustrated with numerical drift-diffusion simulations.[67,83,84] As demonstrated in Figure S23 (Supporting Information), using the well-established drift-diffusion simulation software SCAPS,[85] we could fully reproduce the $J$–$V$ curve of our certified 1 cm$^2$ device using the measured parameters (i.e., $k_2$ and mobilities) as input parameters. Finally, we show that for PM6:Y6 with the reported initial $J_{SC}$ close to 25 mA cm$^{-2}$, a PCE of over 18% is within reach if the recombination coefficient is substantially smaller and the carrier mobility can be increased by one order of

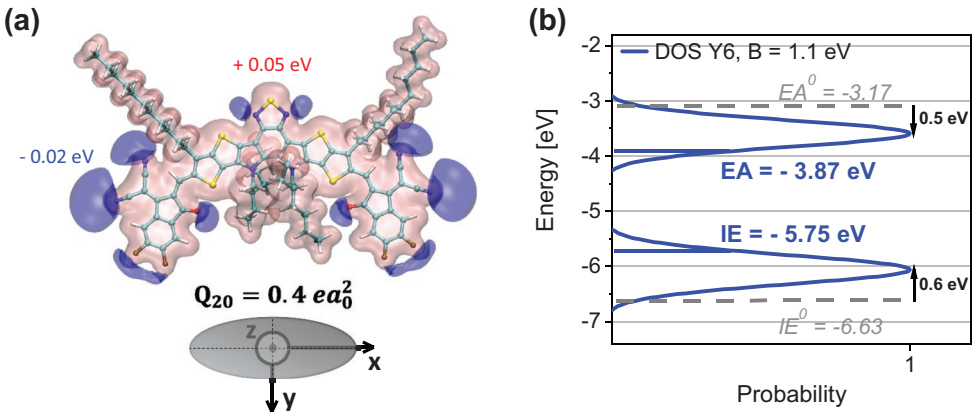


**Figure 4.** a) Isosurfaces of the electrostatic potential of Y6 leading to its large quadrupolar moment, together with the ellipsoid of the quadrupole tensor. See Figure S20 (Supporting Information) for the equivalent calculation of the isosurfaces of the electrostatic potential of PM6. b) Calculated density of states (DOS) for electrons (EA) and holes (IE) in a model crystal of Y6 (see the Supporting Information for the calculation details). The onset of the DOS, evaluated as its maximum plus/minus 2$\sigma$ for (electrons/holes) gives the ionization energy and electron affinity of the Y6 crystal.

magnitude (a summary of all simulation parameters is given in Table S2, Supporting Information).

In summary, we studied free charge generation in inverted PM6:Y6 devices, using a combination of TDCF, EQE, and $V_{OC}$ measurements. We find that CT dissociation is field independent regardless of whether the acceptor, the donor, or the CT state is excited, pointing to a cold free charge generation pathway with a very small dissociation barrier. Temperature-dependent measurements reveal an exceptional small activation energy for CT dissociation of only 6 meV and efficient photocurrent generation down to $T \approx 100$ K. We exclude that charge separation is mainly driven by disorder, given the small $\sigma$ values in the IE and EA and that nongeminate recombination is a nondispersive, purely second-order process. We propose that the large quadrupolar moments of Y6 on a molecular scale, its dimerization in a unit cell, and the specific acceptor–donor–acceptor molecular architecture create an electrostatic bias potential which compensates the Coulomb binding of the charge transfer state, thus enabling barrier-free dissociation of CT states.

## Supporting Information

Supporting Information is available from the Wiley Online Library or from the author.

## Acknowledgements

L.P.-T. and H.Z. contributed equally to this work. A.M. acknowledges postdoctoral support of the Alexander von Humboldt Foundation. Y.Z. acknowledges National Natural Science Foundation of China (21875286). F.G. acknowledges the Swedish Energy Agency Energimyndigheten (Grant No. 2016-010174). D.A. acknowledges funding from the BMBF grant InterPhase and MESOMERIE (FKZ 13N13661, FKZ 13N13656) and the European Union Horizon 2020 research and innovation program "Widening materials models" under Grant Agreement No. 646259 (MOSTOPHOS). D.A. also acknowledges the KAUST PSE Division for hosting his sabbatical in the framework of the Division's Visiting Faculty program. S.S. was supported by a Sofia Kovalevskaya Award from the Alexander von Humboldt Foundation. The authors thank Dr. Rui Zhang, Dr. Martijn Kemerink, and Tanvi Upreti for fruitful discussions.

## Conflict of Interest

The authors declare no conflict of interest.

## Keywords

driving force, non-fullerene acceptors, organic solar cells, photocurrent generation

Received: October 18, 2019
Revised: December 19, 2019
Published online: January 24, 2020

[1] Y. Cui, H. Yao, J. Zhang, T. Zhang, Y. Wang, L. Hong, K. Xian, B. Xu, S. Zhang, J. Peng, Z. Wei, F. Gao, J. Hou, *Nat. Commun.* **2019**, *10*, 2515.
[2] X. Xu, K. Feng, Z. Bi, W. Ma, G. Zhang, Q. Peng, *Adv. Mater.* **2019**, *31*, 1901872.
[3] L. Meng, Y. Zhang, X. Wan, C. Li, X. Zhang, Y. Wang, X. Ke, Z. Xiao, L. Ding, R. Xia, H.-L. Yip, Y. Cao, Y. Chen, *Science* **2018**, *361*, 1094.
[4] J. Yuan, Y. Zhang, L. Zhou, G. Zhang, H.-L. Yip, T.-K. Lau, X. Lu, C. Zhu, H. Peng, P. A. Johnson, M. Leclerc, Y. Cao, J. Ulanski, Y. Li, Y. Zou, *Joule* **2019**, *3*, 1140.
[5] S. Xiong, L. Hu, L. Hu, L. Sun, F. Qin, X. Liu, M. Fahlman, Y. Zhou, *Adv. Mater.* **2019**, *31*, 1806616.
[6] J. Yuan, T. Huang, P. Cheng, Y. Zou, H. Zhang, J. L. Yang, S.-Y. Chang, Z. Zhang, W. Huang, R. Wang, D. Meng, F. Gao, Y. Yang, *Nat. Commun.* **2019**, *10*, 570.
[7] D. Qian, Z. Zheng, H. Yao, W. Tress, T. R. Hopper, S. Chen, S. Li, J. Liu, S. Chen, J. Zhang, X.-K. Liu, B. Gao, L. Ouyang, Y. Jin, G. Pozina, I. A. Buyanova, W. M. Chen, O. Inganäs, V. Coropceanu, J.-L. Bredas, H. Yan, J. Hou, F. Zhang, A. A. Bakulin, F. Gao, *Nat. Mater.* **2018**, *17*, 703.
[8] D. Baran, T. Kirchartz, S. Wheeler, S. Dimitrov, M. Abdelsamie, J. Gorman, R. S. Ashraf, S. Holliday, A. Wadsworth, N. Gasparini, P. Kaienburg, H. Yan, A. Amassian, C. J. Brabec, J. R. Durrant, I. McCulloch, *Energy Environ. Sci.* **2016**, *9*, 3783.
[9] M. Azzouzi, T. Kirchartz, J. Nelson, *Trends Chem.* **2019**, *1*, 49.
[10] R. S. Gurney, D. G. Lidzey, T. Wang, *Rep. Prog. Phys.* **2019**, *82*, 036601.
[11] C. L. Braun, *J. Chem. Phys.* **1984**, *80*, 4157.
[12] T. Unger, S. Wedler, F.-J. Kahle, U. Scherf, H. Bässler, A. Köhler, *J. Phys. Chem. C* **2017**, *121*, 22739.
[13] J. Shi, A. Isakova, A. Abudulimu, M. van den Berg, O. K. Kwon, A. J. Meixner, S. Y. Park, D. Zhang, J. Gierschner, L. Lüer, *Energy Environ. Sci.* **2018**, *11*, 211.
[14] J. Liu, S. Chen, D. Qian, B. Gautam, G. Yang, J. Zhao, J. Bergqvist, F. Zhang, W. Ma, H. Ade, O. Inganäs, K. Gundogdu, F. Gao, H. Yan, *Nat. Energy* **2016**, *1*, 16089.
[15] S. Li, L. Zhan, C. Sun, H. Zhu, G. Zhou, W. Yang, M. Shi, C.-Z. Li, J. Hou, Y. Li, H. Chen, *J. Am. Chem. Soc.* **2019**, *141*, 3073.
[16] H. Yao, Y. Cui, D. Qian, C. S. Ponseca, A. Honarfar, Y. Xu, J. Xin, Z. Chen, L. Hong, B. Gao, R. Yu, Y. Zu, W. Ma, P. Chabera, T. Pullerits, A. Yartsev, F. Gao, J. Hou, *J. Am. Chem. Soc.* **2019**, *141*, 7743.
[17] R. Scholz, R. Luschtinetz, G. Seifert, T. Jägeler-Hoheisel, C. Körner, K. Leo, M. Rapacioli, *J. Phys.: Condens. Matter* **2013**, *25*, 473201.
[18] A. Tang, B. Xiao, Y. Wang, F. Gao, K. Tajima, H. Bin, Z.-G. Zhang, Y. Li, Z. Wei, E. Zhou, *Adv. Funct. Mater.* **2018**, *28*, 1704507.
[19] H. Cha, C.-H. Tan, J. Wu, Y. Dong, W. Zhang, H. Chen, S. Rajaram, K. S. Narayan, I. McCulloch, J. R. Durrant, *Adv. Energy Mater.* **2018**, *8*, 1801537.
[20] K. Nakano, Y. Chen, B. Xiao, W. Han, J. Huang, H. Yoshida, E. Zhou, K. Tajima, *Nat. Commun.* **2019**, *10*, 2520.
[21] H. Tamura, I. Burghardt, *J. Am. Chem. Soc.* **2013**, *135*, 16364.
[22] A. Y. Sosorev, D. Y. Godovsky, D. Y. Paraschuk, *Phys. Chem. Chem. Phys.* **2018**, *20*, 3658.
[23] K. Vandewal, S. Albrecht, E. T. Hoke, K. R. Graham, J. Widmer, J. D. Douglas, M. Schubert, W. R. Mateker, J. T. Bloking, G. F. Burkhard, A. Sellinger, J. M. J. Fréchet, A. Amassian, M. K. Riede, M. D. McGehee, D. Neher, A. Salleo, *Nat. Mater.* **2014**, *13*, 63.
[24] D. Di Nuzzo, L. J. A. Koster, V. S. Gevaerts, S. C. J. Meskers, R. A. J. Janssen, *Adv. Energy Mater.* **2014**, *4*, 1400416.
[25] S. Athanasopoulos, F. Schauer, V. Nádaždy, M. Weiß, F. Kahle, U. Scherf, H. Bässler, A. Köhler, *Adv. Energy Mater.* **2019**, *9*, 1900814.
[26] F. Gao, W. Tress, J. Wang, O. Inganäs, *Phys. Rev. Lett.* **2015**, *114*, 128701.
[27] J. Zhang, A. C. Jakowetz, G. Li, D. Di, S. M. Menke, A. Rao, R. H. Friend, A. A. Bakulin, *J. Mater. Chem. A* **2017**, *5*, 11949.

[28] M. Gerhard, A. P. Arndt, M. Bilal, U. Lemmer, M. Koch, I. A. Howard, *Phys. Rev. B* **2017**, *95*, 195301.
[29] J. Kurpiers, T. Ferron, S. Roland, M. Jakoby, T. Thiede, F. Jaiser, S. Albrecht, S. Janietz, B. A. Collins, I. A. Howard, D. Neher, *Nat. Commun.* **2018**, *9*, 2038.
[30] Y. Dong, H. Cha, J. Zhang, E. Pastor, P. S. Tuladhar, I. McCulloch, J. R. Durrant, A. A. Bakulin, *J. Chem. Phys.* **2019**, *150*, 104704.
[31] J. Benduhn, K. Tvingstedt, F. Piersimoni, S. Ullbrich, Y. Fan, M. Tropiano, K. A. McGarry, O. Zeika, M. K. Riede, C. J. Douglas, S. Barlow, S. R. Marder, D. Neher, D. Spoltore, K. Vandewal, *Nat. Energy* **2017**, *2*, 17053.
[32] F. D. Eisner, M. Azzouzi, Z. Fei, X. Hou, T. D. Anthopoulos, T. J. S. Dennis, M. Heeney, J. Nelson, *J. Am. Chem. Soc.* **2019**, *141*, 6362.
[33] E. Collado-Fregoso, S. N. Pugliese, M. Wojcik, J. Benduhn, E. Bar-Or, L. Perdigón-Toro, U. Hörmann, D. Spoltore, K. Vandewal, J. M. Hodgkiss, D. Neher, *J. Am. Chem. Soc.* **2019**, *141*, 2329.
[34] X.-K. Chen, V. Coropceanu, J.-L. Brédas, *Nat. Commun.* **2018**, *9*, 5295.
[35] S. D. Dimitrov, M. Azzouzi, J. Wu, J. Yao, Y. Dong, P. S. Tuladhar, B. C. Schroeder, E. R. Bittner, I. McCulloch, J. Nelson, J. R. Durrant, *J. Am. Chem. Soc.* **2019**, *141*, 4634.
[36] M. S. Vezie, M. Azzouzi, A. M. Telford, T. R. Hopper, A. B. Sieval, J. C. Hummelen, K. Fallon, H. Bronstein, T. Kirchartz, A. A. Bakulin, T. M. Clarke, J. Nelson, *ACS Energy Lett.* **2019**, *4*, 2096.
[37] M. A. Green, E. D. Dunlop, J. Hohl-Ebinger, M. Yoshita, N. Kopidakis, A. W. Y. Ho-Baillie, *Prog. Photovoltaics Res. Appl.* **2020**, *28*, 3.
[38] K. Vandewal, J. Benduhn, V. C. Nikolis, *Sustainable Energy Fuels* **2018**, *2*, 538.
[39] Y. Wang, D. Qian, Y. Cui, H. Zhang, J. Hou, K. Vandewal, T. Kirchartz, F. Gao, *Adv. Energy Mater.* **2018**, *8*, 1801352.
[40] J. Kurpiers, D. Neher, *Sci. Rep.* **2016**, *6*, 26832.
[41] L. Onsager, *Phys. Rev.* **1938**, *54*, 554.
[42] S. Albrecht, K. Vandewal, J. R. Tumbleston, F. S. U. Fischer, J. D. Douglas, J. M. J. Fréchet, S. Ludwigs, H. Ade, A. Salleo, D. Neher, *Adv. Mater.* **2014**, *26*, 2533.
[43] O. Alqahtani, M. Babics, J. Gorenflot, V. Savikhin, T. Ferron, A. H. Balawi, A. Paulke, Z. Kan, M. Pope, A. J. Clulow, J. Wolf, P. L. Burn, I. R. Gentle, D. Neher, M. F. Toney, F. Laquai, P. M. Beaujuge, B. A. Collins, *Adv. Energy Mater.* **2018**, *8*, 1702941.
[44] S. Chandrabose, K. Chen, A. J. Barker, J. J. Sutton, S. K. K. Prasad, J. Zhu, J. Zhou, K. C. Gordon, Z. Xie, X. Zhan, J. M. Hodgkiss, *J. Am. Chem. Soc.* **2019**, *141*, 6922.
[45] A. J. Moulé, D. Neher, S. T. Turner, *P3HT Revisited – From Molecular Scale to Solar Cell Devices*, Springer, Berlin **2014**, pp. 181–232.
[46] T. M. Clarke, A. M. Ballantyne, J. Nelson, D. D. C. Bradley, J. R. Durrant, *Adv. Funct. Mater.* **2008**, *18*, 4029.
[47] A. A. Bakulin, Y. Xia, H. J. Bakker, O. Inganäs, F. Gao, *J. Phys. Chem. C* **2016**, *120*, 4219.
[48] J. Bergqvist, C. Lindqvist, O. Bäcke, Z. Ma, Z. Tang, W. Tress, S. Gustafsson, E. Wang, E. Olsson, M. R. Andersson, O. Inganäs, C. Müller, *J. Mater. Chem. A* **2014**, *2*, 6146.
[49] A. Melianas, V. Pranculis, Y. Xia, N. Felekidis, O. Inganäs, V. Gulbinas, M. Kemerink, *Adv. Energy Mater.* **2017**, *7*, 1602143.
[50] S. N. Hood, I. Kassal, *J. Phys. Chem. Lett.* **2016**, *7*, 4495.
[51] Y. Puttisong, Y. Xia, X. Chen, F. Gao, I. A. Buyanova, O. Inganäs, W. M. Chen, *J. Phys. Chem. C* **2018**, *122*, 12640.
[52] T. M. Burke, M. D. McGehee, *Adv. Mater.* **2014**, *26*, 1923.
[53] A. Devižis, K. Meerholz, D. Hertel, V. Gulbinas, *Chem. Phys. Lett.* **2010**, *498*, 302.
[54] A. C. Jakowetz, M. L. Böhm, J. Zhang, A. Sadhanala, S. Huettner, A. A. Bakulin, A. Rao, R. H. Friend, *J. Am. Chem. Soc.* **2016**, *138*, 11672.
[55] C. Deibel, T. Strobel, V. Dyakonov, *Phys. Rev. Lett.* **2009**, *103*, 036402.
[56] C. Groves, *Energy Environ. Sci.* **2013**, *6*, 3202.
[57] S. Shoaee, S. Subramaniyan, H. Xin, C. Keiderling, P. S. Tuladhar, F. Jamieson, S. A. Jenekhe, J. R. Durrant, *Adv. Funct. Mater.* **2013**, *23*, 3286.
[58] M. Casalegno, R. Pastore, J. Idé, R. Po, G. Raos, *J. Phys. Chem. C* **2017**, *121*, 16693.
[59] F.-J. Kahle, C. Saller, S. Olthof, C. Li, J. Lebert, S. Weiß, E. M. Herzig, S. Hüttner, K. Meerholz, P. Strohriegl, A. Köhler, *J. Phys. Chem. C* **2018**, *122*, 21792.
[60] O. Rubel, S. D. Baranovskii, W. Stolz, F. Gebhard, *Phys. Rev. Lett.* **2008**, *100*, 196602.
[61] S. Hood, N. Zarrabi, P. Meredith, I. Kassal, A. Armin, *J. Phys. Chem. Lett.* **2019**, *10*, 3863.
[62] N. Felekidis, A. Melianas, M. Kemerink, *Org. Electron.* **2018**, *61*, 318.
[63] H. Bässler, *Phys. Status Solidi* **1993**, *175*, 15.
[64] A. Hofacker, D. Neher, *Phys. Rev. B* **2017**, *96*, 245204.
[65] S. Roland, J. Kniepert, J. A. Love, V. Negi, F. Liu, P. Bobbert, A. Melianas, M. Kemerink, A. Hofacker, D. Neher, *J. Phys. Chem. Lett.* **2019**, *10*, 1374.
[66] J. Kniepert, A. Paulke, L. Perdigón-Toro, J. Kurpiers, H. Zhang, F. Gao, J. Yuan, Y. Zou, V. M. Le Corre, L. J. A. Koster, D. Neher, *J. Appl. Phys.* **2019**, *126*, 205501.
[67] J. Kniepert, I. Lange, N. J. van der Kaap, L. J. A. Koster, D. Neher, *Adv. Energy Mater.* **2014**, *4*, 1301401.
[68] S. M. Hosseini, S. Roland, J. Kurpiers, Z. Chen, K. Zhang, F. Huang, A. Armin, D. Neher, S. Shoaee, *J. Phys. Chem. C* **2019**, *123*, 6823.
[69] T. Kirchartz, J. Nelson, *Phys. Rev. B* **2012**, *86*, 165201.
[70] G. Lakhwani, A. Rao, R. H. Friend, *Annu. Rev. Phys. Chem.* **2014**, *65*, 557.
[71] H. Cha, G. Fish, J. Luke, A. Alraddadi, H. H. Lee, W. Zhang, Y. Dong, S. Limbu, A. Wadsworth, I. P. Maria, L. Francàs, H. L. Sou, T. Du, J. Kim, M. A. McLachlan, I. McCulloch, J. R. Durrant, *Adv. Energy Mater.* **2019**, *9*, 1901254.
[72] K. Jiang, Q. Wei, J. Y. L. Lai, Z. Peng, H. K. Kim, J. Yuan, L. Ye, H. Ade, Y. Zou, H. Yan, *Joule* **2019**, *3*, P3020.
[73] C. Poelking, D. Andrienko, *J. Am. Chem. Soc.* **2015**, *137*, 6320.
[74] C. Poelking, M. Tietze, C. Elschner, S. Olthof, D. Hertel, B. Baumeier, F. Würthner, K. Meerholz, K. Leo, D. Andrienko, *Nat. Mater.* **2015**, *14*, 434.
[75] M. Schwarze, W. Tress, B. Beyer, F. Gao, R. Scholz, C. Poelking, K. Ortstein, A. A. Günther, D. Kasemann, D. Andrienko, K. Leo, *Science* **2016**, *352*, 1446.
[76] M. Schwarze, K. S. Schellhammer, K. Ortstein, J. Benduhn, C. Gaul, A. Hinderhofer, L. Perdigón-Toro, R. Scholz, J. Kublitski, S. Roland, M. Lau, C. Poelking, D. Andrienko, G. Cuniberti, F. Schreiber, D. Neher, K. Vandewal, F. Ortmann, K. Leo, *Nat. Commun.* **2019**, *10*, 2466.
[77] C. Poelking, D. Andrienko, *J. Chem. Theory Comput.* **2016**, *12*, 4516.
[78] G. D'Avino, L. Muccioli, F. Castet, C. Poelking, D. Andrienko, Z. G. Soos, J. Cornil, D. Beljonne, *J. Phys.: Condens. Matter* **2016**, *28*, 433002.
[79] N. B. Kotadiya, A. Mondal, P. W. M. Blom, D. Andrienko, G.-J. A. H. Wetzelaer, *Nat. Mater.* **2019**, *18*, 1182.
[80] D. Abbaszadeh, A. Kunz, N. B. Kotadiya, A. Mondal, D. Andrienko, J. J. Michels, G.-J. A. H. Wetzelaer, P. W. M. Blom, *Chem. Mater.* **2019**, *31*, 6380.
[81] A. Karki, J. Vollbrecht, A. L. Dixon, N. Schopp, M. Schrock, G. N. M. Reddy, T. Nguyen, *Adv. Mater.* **2019**, *31*, 1903868.
[82] H. Mangold, A. A. Bakulin, I. A. Howard, C. Kästner, D. A. M. Egbe, H. Hoppe, F. Laquai, *Phys. Chem. Chem. Phys.* **2014**, *16*, 20329.
[83] L. J. A. Koster, E. C. P. Smits, V. D. Mihailetchi, P. W. M. Blom, *Phys. Rev. B* **2005**, *72*, 085205.
[84] J. Kniepert, I. Lange, J. Heidbrink, J. Kurpiers, T. J. K. Brenner, L. J. A. Koster, D. Neher, *J. Phys. Chem. C* **2015**, *119*, 8310.
[85] M. Burgelman, P. Nollet, S. Degrave, *Thin Solid Films* **2000**, *361*, 527.